Porphyrins on mica: Atomic force microscopy imaging in organic solvents

Honda, Hirotaka
Sasahara, Akira
Onishi, Hiroshi

(Citation)
Colloids and Surfaces A: Physicochemical and Engineering Aspects,561:194-200

(Issue Date)
2019-01-20

(Resource Type)
journal article

(Version)
Accepted Manuscript

(URL)
https://hdl.handle.net/20.500.14094/90005357

Porphyrins on Mica: Atomic Force Microscopy Imaging in Organic Solvents

Hirotaka Honda, Akira Sasahara, Hiroshi Onishi*

Department of Chemistry, Graduate School of Science, Kobe University, Nada, Kobe, Hyogo 657-8501, Japan

*Corresponding author. E-mail address: oni@kobe-u.ac.jp

Abstract

Adsorption of 5,10,15,20-tetraphenyl-21*H*,23*H*-porphyrin cobalt (CoTPP) on mica immersed in organic solvents of 1-hexanol, 1-chlorohexane, and 1-phenyloctane was examined. Flat-lying CoTPP molecules were recognized in topographic images observed by atomic force microscopy. The topographic height of individual porphyrins fluctuated by 0.2 nm in a time scale of 10 s. The height fluctuation was ascribed to two states with and without a solvent molecule trapped in the axial ligand position of the CoTPP. In imaging in phenyloctane, adsorbed CoTPPs were removed by adding 1-hexylamine to the imaging solution. Hexylamine ligands would have occupied the axial position of CoTPP to hinder adsorption. In addition, two-dimensional distribution of force pushing the tip was observed in hexanol to show a layered liquid structure parallel to the mica surface.

Keywords

metalloporphyrin; mica; organic solvent; axial ligand; atomic force microscopy

1. Introduction

Metalloporphyrins provide a class of organometallic compounds with one metal cation in the center coordinated to a planar porphine ligand. They are often active catalysts that are functional in organic solvents. The epoxidation of alkene [1, 2], photosensitization in photochemical hydrogen generation or solar cells [3–7], as well as C–H functionalization (e.g. primary, secondary, tertiary, allylic, and benzylic C–H bonds) in hydroxylation, amination, and alkylation [8, 9], provide well-known applications of metalloporphyrins. By anchoring on solid substrates, the functions of the metalloporphyrins in solution may be transferred onto the solids. In keeping with this idea, a number of studies have been conducted to anchor and characterize porphyrins on substrates [10–12]. Scanning probe microscopy is particularly promising for visualizing the anchored species. Individual porphyrins anchored on conductive materials, such as octaethyl- or tetraphenyl-porphyrin coordinated Co, Ni, Zn, and Mn, have been imaged using scanning tunneling microscopy [13–19]. Atomic force microscopy (AFM) is applicable to porphyrins on insulators placed in a vacuum or in air [20–24]. However, individual porphyrins at liquid–solid interfaces have not yet been visualized by AFM.

In the present study, a cobalt porphyrin was anchored on mica and imaged in organic solvents using AFM in the frequency-modulation mode of force detection. Highly sensitive force detection achieved by this mode enabled us to recognize solvents coordinating to the Co center. Cobalt porphyrins attract attention as catalysts for water oxidation [25], oxidative coupling of phenol derivatives [26], and CO_2 reduction [27]. Figure 1 shows the examined porphyrin, 5,10,15,20-tetraphenyl-21*H*,23*H*-porphyrin cobalt, hereafter referred to as CoTPP. To simulate the realistic environments of catalytic reactions, the anchored CoTPP in three solvents (1-hexanol, 1-chlorohexane, and 1-phenyloctane) was imaged in terms of different coordination strengths to the Co cation center. A more efficient reagent for coordination, 1-hexylamine, was added to the phenyloctane solvent for further examination. Observation in solvents of less efficient coordination, hydrocarbons, was desirable but not conducted due to the limited solubility of CoTPP.

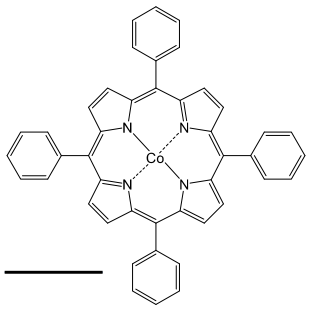

Fig. 1. 5,10,15,20-Tetraphenyl-21*H*,23*H*-porphyrin cobalt (CoTPP) with a scale bar of 0.5 nm.

2. Experimental section

2.1. Materials

5,10,15,20-Tetraphenyl-21*H*,23*H*-porphyrin cobalt (Sigma-Aldrich, >85%), 1-hexanol (Sigma-Aldrich, >99%), 1-chlorohexane (Tokyo Chemical, >95%), 1-phenyloctane (Tokyo Chemical, >98%), and 1-hexylamine (Tokyo Chemical, >99%) were used without purification. A muscovite mica wafer (Furuuchi Chemical, 10 mm × 10 mm) was glued onto a holder and cleaved with scotch tape just before adding the imaging solutions.

2.2. Microscope

Frequency-modulation detection of the tip-surface force was enabled in the imaging solutions by using an SPM-8100FM (Shimadzu) microscope in developing. In topographic imaging, the resonance oscillation of a cantilever is mechanically excited with a constant amplitude of oscillation (A). When a conservative force is applied to the tip at the free end of the oscillating cantilever, the resonance frequency (f) shifts accordingly. The topography of a solid object is traced with regulation of the tip-surface distance by keeping the frequency shift (Δf) constant as a setpoint. Silicon cantilevers (NCH, Nanoworld) with a nominal spring constant (k) of 42 N m^{-1} were backside-coated with gold. The resonant frequency of the cantilever was 130–180 kHz, and the quality factor (Q) of resonance oscillation was 5–10 in the imaging solutions. A solution droplet was put on the mica wafer, and then the cantilever assembly was placed on top. The cantilever was completely immersed in the imaging solution. The droplet on the wafer was open to the environment. Imaging scans were conducted at 298 K in a thermostatic container with Peltier devices. Reproducibility of each measurement was checked and confirmed. A representative set of results is shown in the manuscript.

3. Results and discussion

3.1. Force curves in pristine 1-hexanol

To check and confirm the force sensing ability of our microscope, force curves were observed on a mica-hexanol interface prior to topographic imaging of CoTPP. Figure 2 shows a cross-sectional Δf distribution observed on a plane perpendicular to the mica surface. The oscillating cantilever was scanned vertically from bulk hexanol to the surface. The frequency shift was simultaneously recorded as a function of the vertical coordinate to obtain one Δf–distance curve at one lateral position. The vertical scan aborted when Δf reached a predetermined threshold, +190 Hz, to prevent severe contact with the surface. The tip then laterally shifted and another vertical scan was carried out. The two-dimensional Δf distribution shown in panel (a) was thereby constructed with 256 vertical scans.

The observed Δf distribution is regarded as an approximate force distribution. A repulsive tip–surface force causes a positive frequency shift, though the relation between the force and Δf is nonlinear. The brightest region near the bottom represented the boundary of hexanol and mica. When the tip went down into that region, the repulsive force increased monotonically. Hence, the flat trace of the brightest region shows the topography of mica.

An important feature here is the uneven distribution of force pushing the tip. A few layers of bright and dark colors repeatedly were recognized in hexanol parallel to the mica surface. The layered force distribution is ascribed to a layered density distribution of liquid hexanol. It is natural that hexanol molecules produce a layer in contact with mica not to make vacuum at the interface. Second and possibly third layers appeared on an averaged Δf-distance curve shown in (b). The averaged curve was further converted to a force-distance curve and shown in (c), by applying the scheme proposed by Sader and Jarvis [28]. The distance of the first and second force minima, and that of the first and second force maxima were 1.6 and 1.8 nm, respectively. These distances provide an estimate of layer-to-layer distances in the structured hexanol liquid, while the force cannot be proportional to liquid density [29, 30].

Two earlier force-curve studies [31, 32] reported layer distances, 1.1 and 1.3 nm, on hexanol-mica interfaces. Our layer distance of 1.6–1.8 nm suggested hexanol molecules standing up on the mica surface possibly making a double layers, since the molecule length of an all-trans 1-hexanol should be 0.9 nm. A distinctly smaller layer distance, 0.6 nm, was observed with 1-decanol on graphite and interpreted with flat-lying decanol molecules [33]. The upright orientation of hexanol on mica is probably caused by affinity of the terminal OH to the hydrophilic surface of mica.

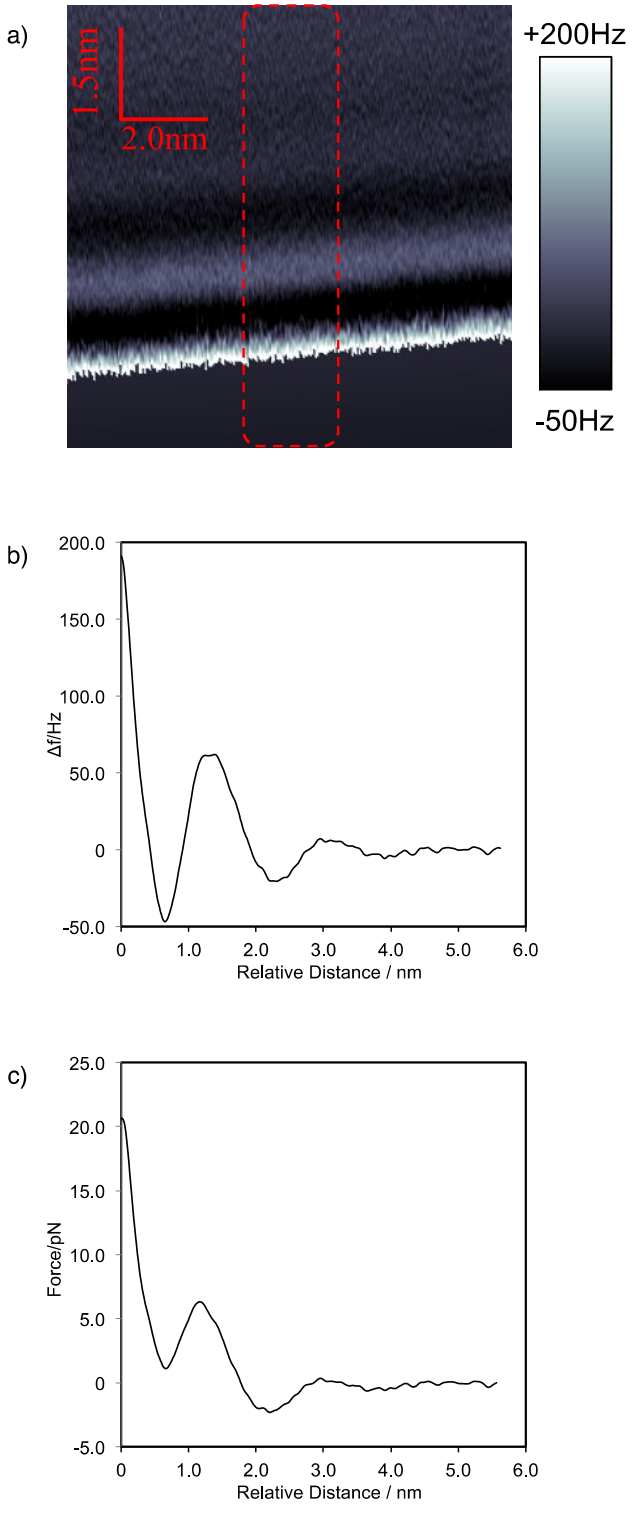

Fig. 2. Force curves on a mica-hexanol interface. A cross-sectional Δf distribution is shown in (a). 56 curves determined in the area marked with the broken lines were averaged and presented in (b). The averaged Δf curve was converted to a force-distance curve (c). Amplitude of cantilever oscillation A: 0.6 nm.

3.2. Topographic imaging in 1-hexanol

Topographic images observed in a hexanol solution of CoTPP (9×10^{-4} mol l^{-1}) are presented in Fig. 3. The frequency-shift setpoint for topographic imaging, +140 Hz, was converted to a repulsive tip-surface force, 17 pN, by using the force curve shown in Fig. 2. Force curves in Fig. 2 and topographic images in Fig. 3 were observed with the same cantilever oscillated by 0.6 nm.

Two topographic images consecutively observed at an interval of 60 s are shown in Figs. 3a and 3b. Protrusions of a uniform lateral size, 10 nm in the full width of half height, are shown. These protrusions were absent on the mica surface immersed in the pristine hexanol solvent (Fig. 3e) and hence were assigned to the adsorbed CoTPP. The uniform lateral size suggests that individual, single molecules accounted for the protrusions. It is known that CoTPP lying flat on the surface is ca. 2 nm in the lateral directions. The larger size observed in the topography can be ascribed to the convolution of the AFM tip apex and the adsorbed CoTPP.

The topographic height distribution of 43 protrusions peaked at 0.3 nm relative to the uncovered mica surface and decreased to 0.5–0.6 nm. As shown in the consecutive images in Figs. 3a and 3b, the two protrusions at the left end on line A–B actually changed in height by 0.2 nm, whereas the two at the right end remained intact. The two states were observed to oscillate back and forth, likely because of equilibration in the hexanol solution. Although the zero height, determined by the topography of mica, was fluctuated, different topography of the two CoTPP states was clearly recognized. The height histogram, on the other hand, presented single peak distributions instead of expected double peak distributions. The authors assume that two peaks with finite peak widths merged into one peak tailing to the large height end in each histogram. The time-averaged population of the low state (0.3 nm height) was larger than that of the high state (0.5 nm height).

The existence of the two states possibly originates from a solvent molecule bound to the Co center with coordination bonding. As described in the literature [34–36], Co(II) centers in porphyrins can be coordinated to one more ligand to complete a five-fold coordination. The Co cation center in our CoTPP is divalent and therefore able to coordinate with one axial ligand. Since AFM imaging was conducted in the hexanol liquid, a hexanol molecule can be coordinately bound to CoTPP. A Co–N(pyridine) bond length of 0.2 nm in a Co(II) porphyrin coordinated to a pyridine ligand was reported [37, 38]. This number agrees with the topographic height difference of the two states observed in Fig. 3. When the OH end of hexanol coordinates

to Co(II), the Co–O distance would be 0.2 nm and the topographic height of the coordinated CoTPP would increase accordingly. The ability to undergo coordinative bonding is indicated by the donor number. The donor numbers of ethanol and 2-ethylhexanol are 20 and 48, respectively [39–41]. Hence, we expect that coordination by 1-hexanol to CoTPP adsorbed on mica would have occurred.

Another possible ligand is O_2 in the hexanol solvent equilibrated with O_2 in air. One earlier STM study [18] reported O_2 adsorption on an octaethyl Co porphyrin with a slightly different porphine ligand fixed on graphite. The molecular adsorption of O_2 was caused by σ donation from O_2 to the d_z^2 orbital of the Co center accompanied by π back-donation [42]. The authors of the STM study assumed that the graphite surface is strongly donating electrons to the Co center, thereby stabilizing the polarized Co-O_2 complex even at RT. In our imaging solutions, CoTPP adsorbed onto mica with no π electron and was free from the electronic enhancement of the binding ability of the Co center with O_2. Coordination by molecular oxygen is thus a less likely explanation for the height increase observed in Fig. 3.

Two CoTPP molecules create a dimer in solutions when their porphyrin planes contact in parallel. When similar stacking occurs, thus creating the two states observed in the present study, the height difference between a monomer and a dimer is expected to be 0.35 nm or more. When two molecules are stacked with π-π interaction in molecular crystals, they are separated by this length [43]. Taking into distortion of porphyrin rings and angles formed between porphyrin rings and phenyl rings, the height difference should increase. Therefore, planer stacking of two CoTPP molecules did not contribute to creation of the two states observed by AFM.

In preceding four paragraphs, the two adsorption states of CoTPP were recognized and their identity was examined on the basis of apparent height in the constant force topography. Heterogeneities in chemical composition and morphology (CoTPP vs mica, and high state vs low state of CoTPP) can affect the apparent height thorough the Hamaker constant and curvature of the scanned objects [44]. In comparing CoTPP with mica, their Hamaker constant and curvature are different and hence the apparent height, 0.3 nm for the low state, should deviate from the absolute height in physical topography. The high and low states of CoTPP, on the other hand, the two quantities are expected to be similar. The apparent height change by 0.2 nm is assigned to topographic difference of the two states of CoTPP.

On the cleaved surface of muscovite mica, $KSi_3Al_3O_{10}(OH)_2$, K cations are thought to partially remain to balance the cationic and anionic charges. A recent study of air-cleaved mica covered with a single-layer of graphene [45] indicated a K cation coverage of 45% relative to

the full occupation of K cations in the crystallographic structure. Some portions of the cleaved surface are occupied by K cations, while the other potions are not. When cleaved mica is immersed in aqueous solutions, the protons, hydroxyls anions, and, potentially, the electrolyte, are adsorbed onto the surface to neutralize the heterogeneity of ionic charges. In our study, cleaved mica wafers were placed in organic solutions free of electrolytes. The charge heterogeneity should be unchanged on the surface. Although CoTPP is a neutral species, the positive charge is localized at the center, and the negative charge is delocalized over the porphyrin ring. The uneven charge distribution in each CoTPP induces an electrostatic attractive interaction with the heterogeneously charged mica surface.

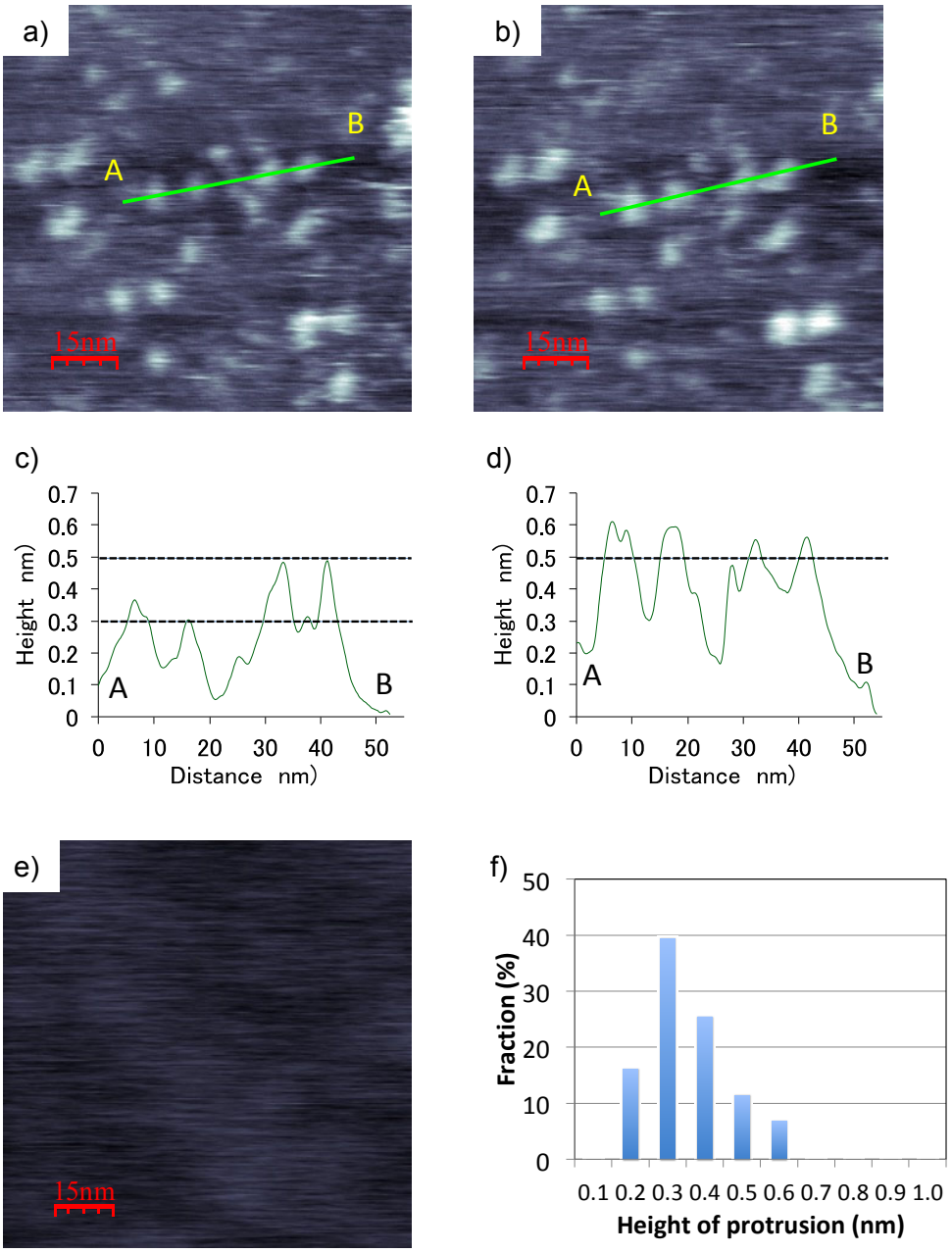

Fig. 3. Topography observed in the hexanol solution of CoTPP. Two images consecutively observed at an interval of 60 s are shown in (a) and (b). A–B cross sections of the two images are respectively shown in (c) and (d). Image (e) was observed in pristine hexanol. A height histogram of 43 protrusions in (a) is shown in (f). Amplitude of cantilever oscillation A: 0.6 nm. Frequency-shift setpoint: +140 Hz.

3.3. Imaging in 1-chlorohexane

CoTPP was dissolved in chlorohexane and then adsorbed onto mica. Topographic images were observed in the 1×10^{-3} mol l^{-1} solution (shown in Fig. 4). Panel (a) presents a wide-area image of a 100 nm square. A number of protrusions appeared on the flat substrate. The height distribution of the protrusions shown in (b) peaked at 0.3 nm. A finite distribution appeared at heights larger than 0.7 nm in the histogram. These particular protrusions would be assigned to aggregated CoTPP instead of single flat-lying porphyrins.

Three magnified images consecutively observed at intervals of 20 s are shown in (c)–(e). The topographic height of protrusion A was observed to change from (c) 0.5, to (d) 0.3, and then return to (e) 0.5 nm. The height of protrusion B remained at 0.5 nm in the three images. The fluctuated height of A was interpreted to result from a chlorohexane molecule being trapped and released at the axial position of CoTPP. The height changes of ±0.2 nm were similar to those observed in the solvent 1-hexanol. Topographic changes resulting from solvent coordination were still observed, although the coordination ability of 1-chlorohexane was expected to be less than that of hexanol. The donor number of chloroform is 4 [46].

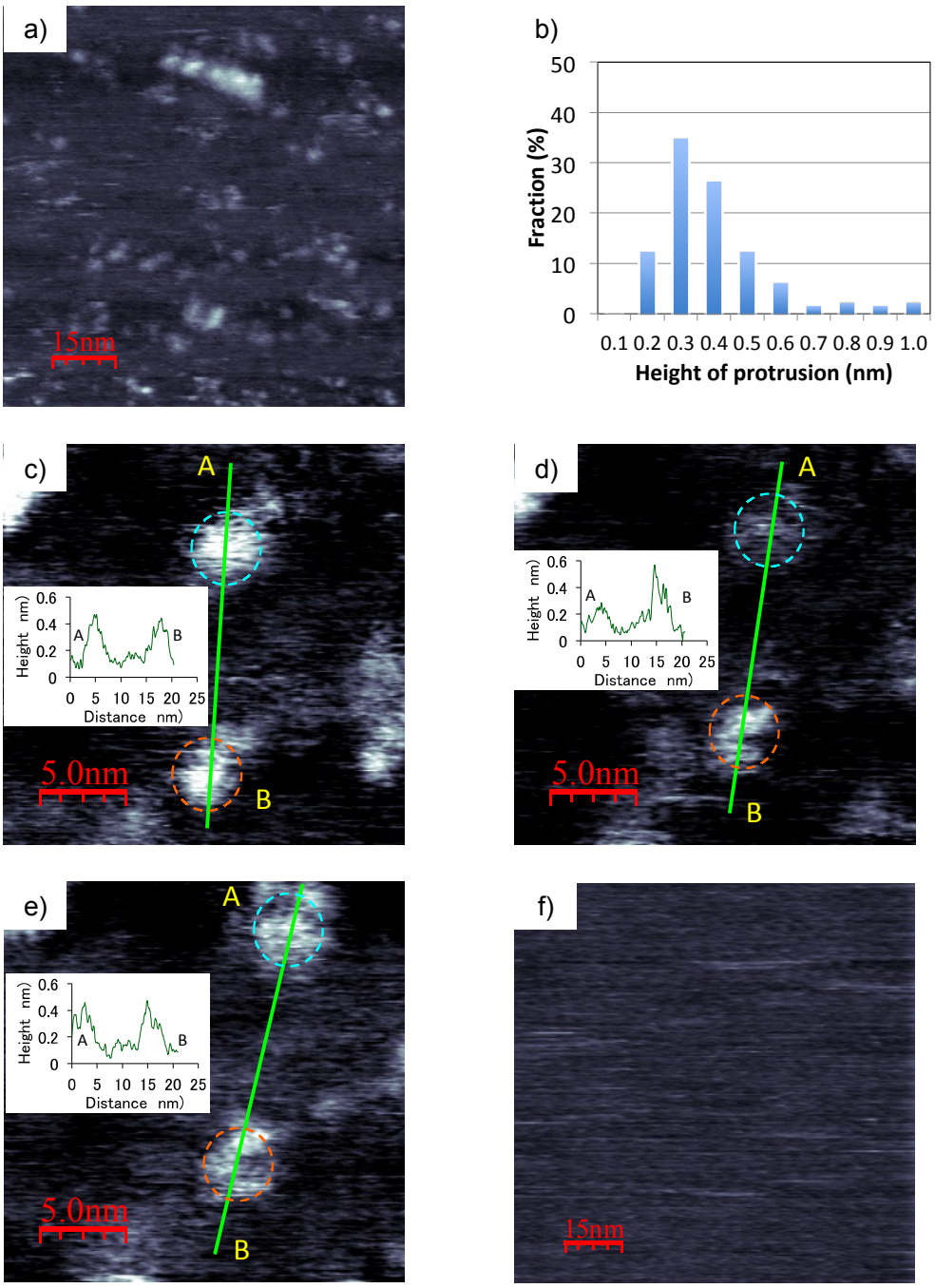

Fig. 4. Topography observed in the chlorohexane solution of CoTPP. The height histogram (N = 129) for (a) is shown in (b). Three images consecutively observed at an interval of 20 s are shown in (c)–(e). Image (f) was observed in pristine chlorohexane. Amplitude of cantilever oscillation *A*: 0.6 nm. Frequency-shift setpoint: +120 Hz. A–B cross sections are shown in the insets.

3.4. Imaging in 1-phenyloctane with and without 1-hexylamine

In this subsection, the C_6 alkane terminated with an amino group is compared with hexanol and chlorohexane. Alkylamines are good ligands to metal cation centers, as indicated by the large donor number of ethylamine, 55 [39–41]. Imaging scans were conducted in a 1-phenlyoctane solution of CoTPP (1×10^{-3} mol l^{-1}) in the presence and absence of hexylamine. Phenyloctane was used as a solvent because of its weak coordination ability.

Figure 5a shows a topographic image observed in the solution with no hexylamine. More protrusions than those in hexanol or chlorohexane solvent appeared and almost covered the mica surface. It was thus not easy to separately recognize individual adsorbed molecules. The increased coverage in phenyloctane is ascribed to the least polar property of this compound among the solvents examined in the present study. CoTPP possesses an electric quadrupole moment caused by the cation center and anion ligand. Depositing CoTPP induces enthalpy gain on the highly polar surface of mica. The enthalpy gain per CoTPP molecule should be larger in a less polar solvent.

With the addition of hexylamine (0.1 mol l^{-1}), the protrusions were removed from the surface. One or two hexylamine ligands occupied the axial position; hence, the coordinated CoTPP lost affinity with the mica surface because of the increased electronic density on the Co cation center and/or steric hindrance induced by the ligands.

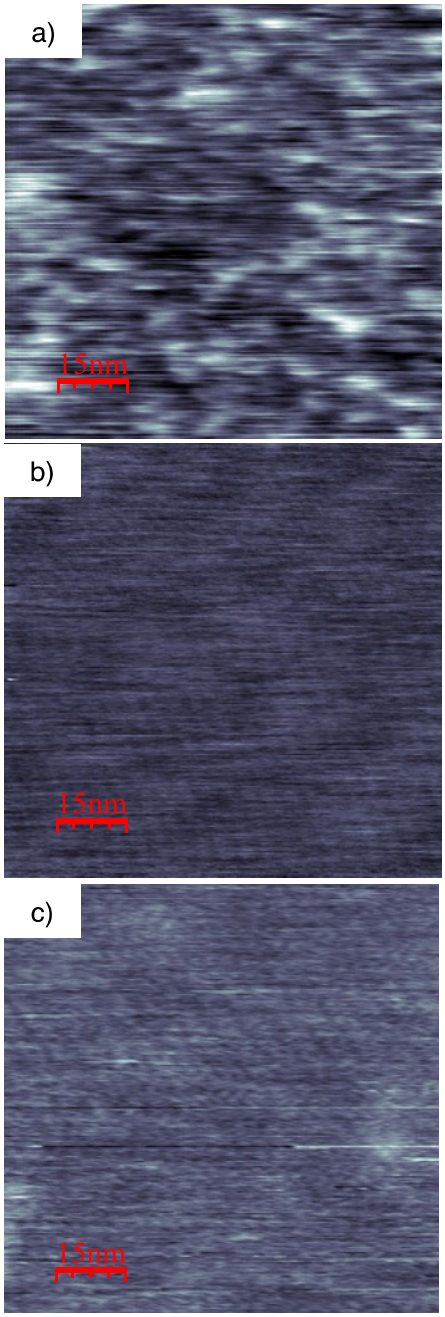

Figure 5. Topography observed in the phenyloctane solutions of CoTPP. Images (a) and (b) were observed in the absence and presence of hexylamine. Image (c) was observed in pristine phenyloctane. Amplitude of cantilever oscillation A: 0.6 nm. Frequency-shift setpoint: +200 Hz.

4. Conclusions

A Co(II)-centered porphyrin, CoTPP, was adsorbed on air-cleaved mica surfaces in three organic solvents: 1-hexanol, 1-chlorohexane, and 1-phenyloctane. The adsorbed porphyrin molecules were individually imaged by constant frequency-shifted topography determined by

frequency-modulation AFM. In the hexanol and chlorohexane solutions of CoTPP, two states of adsorption were identified and assigned to a flat-lying CoTPP molecule in the presence or absence of a solvent molecule that is trapped in the axial ligand position directed toward the solution. This trapping and releasing process were observed in consecutive imaging scans. Upon addition of 1-hexylamine to the phenyloctane solution, CoTPP was desorbed and coordinated with this compound in the solution.

Acknowledgment. This study was supported by Special Coordination Funds for Promoting Science and Technology, Creation of Innovation Centers for Advanced Interdisciplinary Research Areas (Innovative Bioproduction, Kobe) and JSPS KAKENHI grant number JP16H02250.

References

[1] B. S. Lane, K. Burgess, Metal-Catalyzed Epoxidations of Alkenes with Hydrogen Peroxide, Chem. Rev. 103 (2003) 2457-2473.

[2] Q.-H. Xia, H.-Q. Ge, C.-P. Ye, Z.-M. Liu, K.-X. Su, Advances in Homogeneous and Heterogeneous Catalytic Asymmetric Epoxidation, Chem. Rev. 105 (2005) 1603-1662.

[3] W. M. Campbell, A. K. Burrell, D. L. Officer, K. W. Jolley, Porphyrins as light harvesters in the dye-sensitized TiO_2 solar cell, Coor. Chem. Rev. 348 (2004) 1363-1379.

[4] J. R. Darwent, P. Douglas, A. Harriman, G. Porter, M.-C. Richoux, Metal Phthalocyanines and Porphyrins as Photosensitizers for Reduction of Water to Hydrogen, Coor. Chem. Rev. 44 (1982) 83-126.

[5] A. J. Esswein, D. G. Nocera, Hydrogen Production by Molecular Photocatalysis, Chem. Rev. 107 (2007) 4022-4047.

[6] L.-L. Li, E. W.-G. Diau, Porphyrin-sensitized solar cells, Chem. Soc. Rev. 42 (2013) 291-304.

[7] K. Ladomenou, M. Natali, E. Iengo, G. Charalampidis, F. Scandola, A. G. Coutsolelos, Photochemical hydrogen generation with porphyrin-based systems, Coor. Chem. Rev. 304-305 (2015) 38-54.

[8] C.-M. Che, V. K.-Y. Lo, C.-Y. Zhou, J.-S. Huang, Selective functionalisation of saturated C–H bonds with metalloporphyrin catalysts, Chem. Soc. Rev. 40 (2011) 1950-1975.

[9] H. Lu, X. P. Zhang, Catalytic C–H functionalization by metalloporphyrins: recent developments and future directions, Chem. Soc. Rev. 40 (2011) 1899-1909.

[10] K. Sugawa, T. Tamura, H. Tahara, D. Yamaguchi, T. Akiyama, J. Otsuki, Y. Kusaka, N. Fukuda, H. Ushijima, Metal-Enhanced Fluorescence Platforms Based on Plasmonic Ordered Copper Arrays: Wavelength Dependence of Quenching and Enhancement Effects, ACS Nano 7 (2013) 9997-11010.

[11] A. K. D. de Freitas Castro, F. Wypych, A. Antonangelo, K. M. Mantovani, A. Bail, G. M. Ucoski, K. J. Ciuffi, T. E. Cintra, S. Nakagaki, Selective oxidation catalysts obtained by immobilization of iron(III) porphyrins on thiosalicylic acid-modified Mg-Al layered double hydroxides, J. Colloid Interface Sci. 478 (2016) 374-383.

[12] L. Zeininger, F. Lodermeyer, R. D. Costa, D. M. Guldi, A. Hirsch, Hydrogen bonding mediated orthogonal and reversible self-assembly of porphyrin sensitizers onto TiO_2 nanoparticles, Chem. Commun. 52 (2016) 8842-8845.

[13] B. Hulsken, R. van Hameren, J. W. Gerritsen, T. Khoury, P. Thordarson, M. J. Crossley, A. E. Rowan, R. J. M. Nolte, J. A. A. Elemans, S. Speller, Real-time single-molecule imaging of oxidation catalysis at a liquid–solid interface, Nat. Nanotech. 106 (2007) 285-289.

[14] T. Kawamoto, S. Yoshimoto, Tuning Porphyrin Assembly and Electrochemical Catalytic Activity with Halogen Substituents, Langmuir 31 (2015) 11532-11538.

[15] A. Bhattarai, K. Marchbanks-Owens, U. Mazur, K. W. Hipps, Influence of the Central Metal Ion on the Desorption Kinetics of a Porphyrin from the Solution/HOPG Interface, J. Phys. Chem. C 120 (2016) 18140-18150.

[16] A. Bhattarai, U. Mazur, K. W. Hipps, Desorption Kinetics and Activation Energy for Cobalt Octaethylporphyrin from Graphite at the Phenyloctane Solution−Graphite Interface: An STM Study, J. Phys. Chem. C 119 (2015) 9386-9394.

[17] D. den Boer, M. Li, T. Habets, P. Iavicoli, A. E. Rowan, R. J. M. Nolte, S. Speller, D. B. Amabilino, S. D. Feyter, J. A. A. W. Elemans, Detection of different oxidation states of individual manganese porphyrins during their reaction with oxygen at a solid/liquid interface, Nat. Chem. 5 (2013) 621-627.

[18] B. A. Friesen, A. Bhattarai, U. Mazur, K. W. Hipps, Single Molecule Imaging of Oxygenation of Cobalt Octaethylporphyrin at the Solution/Solid Interface: Thermodynamics from Microscopy, J. Am. Chem. Soc. 134 (2012) 14897-14904.

[19] Q. Ferreira, L. Alcácer, J. Morgado, Stepwise preparation and characterization of molecular wires made of zinc octaethylporphyrin complexes bridged by 4, 4'-bipyridine on HOPG, Nanotech. 22 (2011) 435604-435610.

[20] V. Snitka, M. Rackaitis, R. Rodaite, Assemblies of $TPPS_4$ porphyrin investigated by TEM, SPM and UV–vis spectroscopy, Sens. Actuators B 109 (2005) 159-166.

[21] Y. Wu, P. Ma, S. Liu, Y. Chen, Amphiphilic unsymmetrically substituted porphyrin zinc derivatives: synthesis, aggregation behavior of the self-assembled films and NO_2 sensing properties, New J. Chem. 40 (2016) 3323-3329.

[22] V. V. Korolkov, S. A. Svatek, A. Summerfield, J. Kerfoot, L. Yang, T. Taniguchi, K. Watanabe, N. R. Champness, N. A. Besley, P. H. Beton, van der Waals-Induced Chromatic Shifts in Hydrogen-Bonded Two-Dimensional Porphyrin Arrays on Boron Nitride, ACS Nano 9 (2015) 10347-10355.

[23] B. Mao, D. G. Calatayud, V. Mirabello, B. J. Hodges, J. A. R. Martins, S. W. Botchway, J. M. Mitchels, S. I. Pascu, Interactions between an Aryl Thioacetate-Functionalized Zn(II) Porphyrin and Graphene Oxide, Adv. Funct. Mater. 26 (2016) 687-697.

[24] F. Albrecht, F. Bischoff, W. Auwärter, J. V. Barth, J. Repp, Direct Identification and Determination of Conformational Response in Adsorbed Individual Nonplanar Molecular Species Using Noncontact Atomic Force Microscopy, Nano Lett. 16 (2016) 7703-7709.

[25] D. K. Dogutan, Jr. R. McGuire, D. G. Nocera, Electocatalytic Water Oxidation by Cobalt(III) Hangman β-Octafluoro Corroles, J. Am. Chem. Soc. 133 (2011) 9178-9180.

[26] Q. Jiang, W. Sheng, M. Tian, J. Tang, C. Guo, Cobalt(II)–Porphyrin-Catalyzed Aerobic Oxidation: Oxidative Coupling of Phenols, Eur. J. Org. Chem. 10 (2013) 1861-1866.

[27] G. F. Manbeck, E. Fujita, A Review of Iron and Cobalt Porphyrins, Phthalocyanines and Related Complexes for Electrochemical and Photochemical Reduction of Carbon Dioxide, J. Porphyrins Phtalocyanines 19 (2015) 45-64.

[28] J. E. Sader, S. P. Jarvis, Accurate formulas for interaction force and energy in frequency modulation force spectroscopy, Appl. Phys. Lett. 84 (2004) 1801-1803.

[29] M. Watkins, B. Reischl, A simple approximation for forces exerted on an AFM tip in liquid, J. Chem. Phys. 138 (2013) 154703.

[30] K. Amano, K. Suzuki, T. Fukuma, O. Takahashi, H. Onishi, The Relationship between Local Liquid Density and Force Applied on a Tip of Atomic Force Microscope: A Theoretical Analysis for Simple Liquids, J. Chem. Phys. 139 (2013) 224710.

[31] Y. Kanda, S. Iwasaki, K. Higashitani, Adhesive Force between Hydrophilic Surfaces in Alcohol–Water Solutions, J. Coll. Interface Sci. 216 (1999) 394-400.

[32] V. Franz, H.-J. Butt, Confined Liquids: Solvation Forces in Liquid Alcohols between Solid Surfaces, J. Phys. Chem. B 106 (2002) 1703-1708.

[33] T. Hiasa, K. Kimura, H. Onishi, Cross-Sectional Structure of Liquid 1-Decanol over Graphite, J. Phys. Chem. C 116 (2012) 26475-26479.

[34] D. Lexa, J. M. Saveant, The electrochemistry of vitamin B_{12}, Acc. Chem. Res. 16 (1983) 235-243.

[35] K. Kadish, L. A. Bottomley, D. Beroiz, Reactions of Pyridine with a Series of Para-substituted Tetraphenylporphyrincobalt and -iron Complexes, Inorg. Chem. 17 (1978) 1124-1129.

[36] D. Achey, S. Ardo, G. J. Meyer, Increase in the Coordination Number of a Cobalt Porphyrin after Photo-Induced Interfacial Electron Transfer into Nanocrystalline TiO_2, Inorg. Chem. 51 (2012) 9865-9872.

[37] J. Li, B. C. Noll, A. G. Oliver, G. Ferraudi, A. G. Lappin, W. R. Scheidt, Oxygenation of Cobalt Porphyrinates: Coordination or Oxidation?, Inorg. Chem. 49 (2010) 2398-2406.

[38] J. S. Summers, J. L. Petersen, A. M. Stolzenberg, Comparison of the Structures of the Five-Coordinate Cobalt(II)Pyridine, Five-Coordinate Cobalt(III) Methyl, and Six-Coordinate Cobalt(III) Methyl Pyridine Complexes of Octaethylporphyrin, J. Am. Chem. Soc. 116 (1994) 7189-7195.

[39] V. Gutmann, Empirical parameters for donor and acceptor properties of solvents, Electrochim. Acta 21 (1976) 661-670.

[40] V. Gutmann, The Donor-Acceptor Approach to Molecular Interactions, Springer (1978).

[41] E. Radzyminska-Lenarcik, Influence of the Solvent Donor Number on the O/W Partition Ratio of Cu(II) Complexes of 1,2-Dialkylimidazoles, Chem. papers 65 (2011) 226-232.

[42] D. V. Stynes, H. C. Stynes, B. R. James, J. A. Ibers, Thermodynamics of Ligand and Oxygen Binding to Cobalt Protoporphyrin IX Dimethyl Ester in Toluene Solution, J. Am. Chem. Soc. 95 (1973) 1796-1801.

[43] D. E. Jazen, K. Patel, D. G. VanDerveer, G. J. Grant, π-π Interactions in diimine Pt(II) complexes with thiacrown ligands: The crystal structure of (1,4,7-trithiacyclononane) (3,4,7,8-tetramethyl-1,10-phenanthroline) platinum(II) hexafluorophosphate, J. Chem. Crystallogr. 36 (2006) 83-91.

[44] C.-Y. Lai, S. Sergio, M. Chiesa, General interpretation and theory of apparent height in dynamic atomic force microscopy, RSC Adv. 5 (2015) 80069-80075.

[45] P. Bampoulis, K. Sotthewes, M. H. Siekman, H. J. W. Zandvliet, B. Poelsema, Graphene Visualizes the Ion Distribution on Air-Cleaved Mica, Sci. Rep. 7 (2017) 43451.

[46] F. Cataldo, A Revision of the Gutmann Donor Numbers of a Series of Phosphoramides

Including TEPA, Eur. Chem. Bull. 4 (2015) 92-97.